ELSEVIER

Contents lists available at ScienceDirect

Journal of Magnetism and Magnetic Materials

journal homepage: www.elsevier.com/locate/jmmm





Artifacts in magnetic force microscopy of histological sections

Kevin J. Walsh ^a, Owen Shiflett ^b, Stavan Shah ^c, Theodore Renner ^c, Nicholas Soulas ^b, Douglas Scharre ^d, Dana McTigue ^e, Gunjan Agarwal ^{a,b,*}

- ^a Biophysics Program, The Ohio State University, Columbus, OH 43210, USA
- ^b Department of Mechanical and Aerospace Engineering, The Ohio State University, Columbus, OH 43210, USA
- ^c Department of Biomedical Engineering, The Ohio State University, Columbus, OH 43210, USA
- d Division of Neurology, The Ohio State University, Columbus, OH 43210, USA
- ^e Department of Neuroscience, The Ohio State University, Columbus, OH 43210, USA

ARTICLE INFO

Keywords: Magnetic force microscopy Ferritin Iron Spleen Brain

ABSTRACT

Detection of iron-oxide nanoparticles in biological samples has widespread applications. Iron can be naturally present in biological tissues as physiological ferrihydrite particles of ferritin(iron) or as biogenic magnetite nanoparticles in certain neurodegenerative pathologies. In our previous studies, we had reported how magnetic force microscopy (MFM) can be used to map iron deposits in tissue sections in a label-free manner. In this study, to improve the efficiency of MFM for histological analysis, we explored the effect of increasing scan rate. Our results show how MFM images of tissue sections can be contaminated with artifacts due to topographical crosstalk, especially at higher scan rates. These artifacts were observed in rodent spleen as well as in sections of brain tissue obtained from patients with Alzheimer's Disease. Our results show how topographical cross talk can make it challenging to unambiguously detect histological iron via MFM. Multimodal approaches can help overcome some of these limitations.

1. Introduction

Ferritin is the largest iron-storage protein in the mammalian body comprising of a \sim 5 to 8 nm iron-oxide core in the form of superparamagnetic Fe³⁺ rich ferrihydrite [1]. However, under certain pathological conditions, alternate composition (e.g., Fe²⁺ rich magnetite) has also been reported which can significantly impact its magnetic properties. Current techniques to spatially map iron in tissue sections exploit its chemical composition. These include the Perls or Turnbull's staining to detect Fe^{3+} or Fe^{2+} and analytical electron microscopy to detect the X-ray spectral signature of iron. While these techniques have progressed our understanding of both physiological and pathological iron, there remain challenges when attempting to characterize biological deposits. These include mismatch of iron distribution ascertained using magnetism based and chemical detection techniques. Further, our ability to simultaneously ascertain the particle size, density, oxidative state, and biochemical environment of iron deposits remains limited. In this regard, techniques which can spatially map biological iron in tissue sections via its magnetic properties and are compatible with routine histological staining can be particularly attractive [2].

Magnetic force microscopy (MFM) is a scanning probe microscopy-based technique which enables spatial mapping of magnetic domains on a sample surface [3]. In its most conventional format, the MFM technique employs a magnetically coated probe to scan a sample in the non-contact or dynamic mode of atomic force microscopy (AFM). This method involves tracking the sample topography in which the probe directly touches the sample. Thereafter interleaved scans at various lift heights (z) above the topographic height are obtained to detect the long-range magnetic forces present between the MFM probe and magnetic domains on the sample. In the case of superparamagnetic particles, the MFM probe is used to both induce as well as detect magnetic moments in the particles in a label-free manner.

Although MFM was initially used to characterize solid-state devices (e.g. recording media in hard drives), recent years have witnessed a growing use of MFM to study various kinds of magnetic nanoparticles [4–6]. For superparamagnetic nanoparticles, MFM has been useful to evaluate the magnetic moment [7,8], magnetic anisotropy and domains [9,10], magnetization curves [11], and the effect of particle aggregation [12,13]. Applications of MFM have also extended to evaluate biological samples [14] such as ferritin proteins [15,16], cells labeled with

^{*} Corresponding author at: E503, Scott Laboratory, 201 W19th Ave, Columbus, OH 43210, USA. *E-mail address:* agarwal.60@osu.edu (G. Agarwal).

magnetic particles [17], and endogenous magnetic (iron) deposits in bacteria [18,19] and in mammalian tissues [20,21].

In our previous study on rodent spleen (a tissue well-established to consist of ferritin(iron) rich lysosomes) we had reported how MFM could yield features with negative phase shifts in regions corresponding to Perls staining with little to no signal in other regions [20]. The size of these features corresponded to that of ferritin-rich lysosomes present in the splenic macrophages. However, the need to perform interleave modes at multiple lift heights can be time consuming. In this study, to improve the efficiency of MFM experiments, we examined the effect of increasing the scan rate. Our investigations reveal that MFM images of biological tissue sections can be contaminated with artifacts arising due to topographical cross-talk. We elucidate the presence of scan-rate dependent artifacts in MFM images of rodent spleen as well as human brain tissue. Taken together, a multimodal analysis coupling MFM with other modalities is ideally suited to unambiguously identify iron deposits in tissue sections.

2. Materials and methods

2.1. Tissue procurement and processing

Rodent spleen: All animal procedures were performed in accordance with and after approval by the Ohio State University (OSU) Institutional Animal Care and Use Committee (IACUC). Spleen was extracted from adult female Sprague Dawley rats (n = 3) after euthanasia. Small segments (\sim 3 mm in size) of spleen were dissected and fixed in 4% paraformaldehyde for 48 h.

Brain tissue: Coronal slices (\sim 2 cm thick), including the hippocampus from Alzheimer's disease (AD) brain tissue (n = 3) was procured from the Buckeye Brain Bank (BBB) at OSU. These samples have been histologically pre-classified as Braak V or VI using the National Institute of Aging-Alzheimer's Association ABC Scoring system [22,23]. The AD brain was collected 5–48 h postmortem, sliced and frozen (-80 °C) without the use fixatives. For histological analysis, small segments (\sim 3 mm in size) of the hippocampus from AD brain tissue were dissected and fixed (in 4% paraformaldehyde) for 48 h. Similarly preserved, control non-AD brain tissue was obtained from age and gender matched subjects through the Comprehensive Human Tissue Network program at OSU.

After fixation, all tissue segments were rinsed with phosphate buffer solution (PBS), embedded in optimal cutting temperature (OCT) medium for two hours at room temperature and flash frozen in liquid nitrogen. The OCT-embedded tissue blocks were sectioned using a HM 550 cryostat (Microm) at 6 μm thickness and placed on Superfrost Plus Microscope slides (Fisher Scientific). At the time of use, the sections were rinsed in PBS, followed by an hour wash in dH2O and air dried overnight at 4 $^{\circ}C$.

Another set of rodent spleen tissue segments were fixed in 2% glutaraldehyde, dehydrated, resin embedded, and thin-sectioned for transmission electron microscopy (TEM) as described earlier [20]. For MFM analysis, thicker sections (500 nm) of the resin embedded tissue were sectioned onto glass coverslips. Histochemical staining for iron was performed on these sections by using a modified Perls staining method [24]. Briefly, the sections were incubated in a 1:1 mixture of 10% ferrocyanide and 10% HCl at 60 $^{\circ}$ C, with the ferrocyanide mixture replaced after thirty minutes of incubation. After 1 h of incubation, the sections were rinsed thoroughly three times with distilled water and allowed to air dry. The sections were imaged for Perls iron staining using the Zeiss Observer light microscope.

2.2. Magnetic force microscopy

MFM imaging was performed using a Multimode AFM equipped with a Nanoscope IIIa Controller (Bruker) [20] or the Bruker Resolve AFM [25] coupled to a Zeiss Observer light microscope. Magnetically coated high-moment MFM probes (ASYMFMHM, Asylum Research) and non-

magnetic AFM probes (NSC15, MikroMasch) were used to scan the samples in the tapping mode. Various scan rates ranging from 0.5 to 5 Hz (at 256 lines per scan) were utilized. Topographic height images (in main scan) and phase images (in the interleaved lift mode) were acquired at lift heights (z) ranging from 20 to 100 nm. The topographic roughness (Ra) from height images, magnitude of phase (ϕ) and size (area) of regions with a negative phase shift were analyzed by using the NanoScope Analysis software. Measurements were performed on at least n=10 regions with negative phase shift per sample type. Unpaired student t-tests assuming equal variances were performed to determine statistical significance (p less than 0.01).

3. Results

In an effort to improve the efficiency of MFM data acquisition for histological analysis, we experimented with scan rates higher than our previously used values of 1 Hz (@ 256 lines/scan). We used OCT embedded rodent spleen tissue as a test sample as we have previously demonstrated how it yields MFM signals (with negative phase shift) as well as comprises of regions which are devoid of MFM signal. As shown in Fig. 1a, by using our previously used scan rate of 1 Hz (and a lift height of 30 nm), we could identify a region devoid of MFM signal. However, upon increasing the scan rate above 1.5 Hz, features with negative phase shifts started appearing in the very same region. Both the size (area) as well as the number of these features increased with increasing scan rates. At scan rates approaching 5 Hz, the area of these features was often $> 2 \mu m^2$ (larger than lysosomes). Examination of the topographic height, amplitude and phase images revealed that these features were artifacts which typically corresponded to topographical changes of the sample. Interestingly no significant differences were observed in the topographical images of the same region at 1 Hz and 2 Hz (as seen in Fig. 1a) or in the surface roughness of the height images at various scan rates (Fig. 1b). We had previously reported how the size of negative phase shift regions in MFM images of spleen tissue (obtained at 1 Hz) corresponded to that of ferritin(iron) rich lysosomes. We therefore compared the area and magnitude of the negative phase shift regions obtained at 1 Hz and 2 Hz. As shown in Fig. 1c, the size of these regions was significantly larger at 2 Hz. The magnitude of the phase signal was similar at both 1 and 2 Hz (Fig. 1d) and the signal persisted at lift heights > 30 nm for both scan rates (data not shown).

To examine if scan-rate dependent artifacts persist across MFM analysis of other tissues, we analyzed OCT embedded brain tissue sections obtained posthumously from the hippocampus of subjects with or without AD. As shown in Fig. 2a, MFM images of the AD brain failed to show regions with a negative phase shift at typically used scan rates of 1 Hz and a lift height, z = 30 nm. However, upon increasing the scan rate, artifacts with a negative (as well as positive) phase shift were frequently observed in these samples typically corresponding to changes in the sample topography. Consistent with our observation on spleen tissue, the size and frequency of these artifacts increased with increasing scan rates. A lift-height dependence indicated that the phase signal persisted in these artifacts even at lift heights of 100 nm. These scan rate dependent artifacts were also observed in non-AD brain tissue (Fig. 2b) and when using a non-magnetic AFM probe on the AD brain tissue (Fig. 2c). To confirm that these were artifacts and did not correspond to iron deposits, we performed Perl's iron staining, but failed to detect a discernable amount of iron in the sections analyzed (data not shown). To ascertain if the artifacts were correlated to topographical surface roughness of the sample, we compared the surface roughness (at a fixed scan size) as well as the size and magnitude of the signal in the artifacts obtained from rodent spleen and AD tissues (Fig. 2d-f). The AD tissue had a slightly higher surface roughness than that of spleen tissue. However, the size and magnitude of the negative phase signal at 2 Hz was similar across tissue types.

In an effort to reduce surface roughness, we utilized 500 nm thick sections of resin-embedded tissue, (typically used for TEM). As

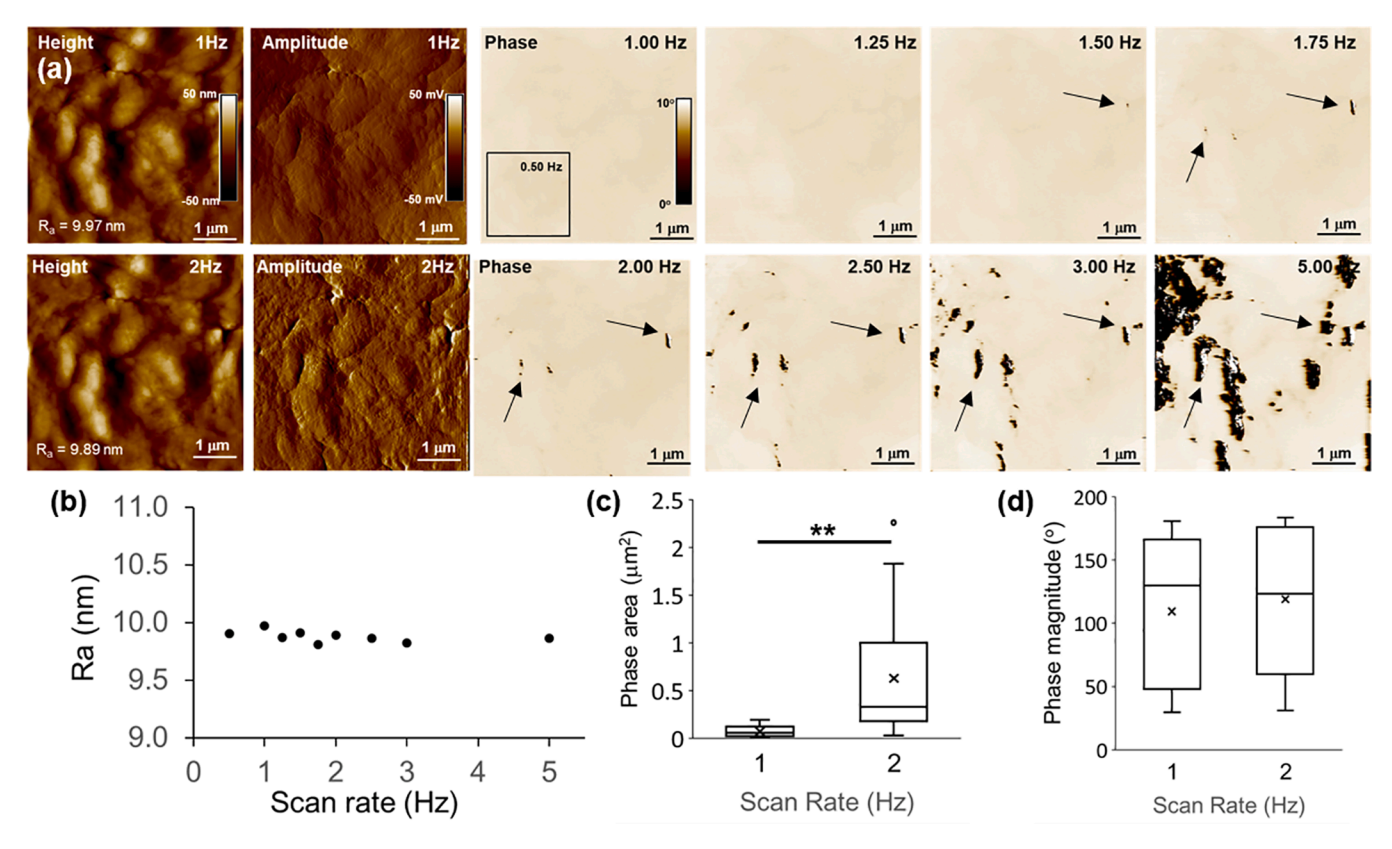


Fig. 1. (a) Sections of OCT-embedded rodent spleen imaged using a MFM probe at various scan rates as indicated. The height and amplitude images were acquired in the main scan while phase images were obtained at a lift height of 30 nm in the interleave mode. Regions with negative phase shift (arrows) start appearing in phase images at scan rates of 1.5 Hz and higher. (b) The surface roughness (R_a) of the height images does not significantly change with increasing scan rate. Quantitative analysis of the (c) area and (d) magnitude of phase shift obtained from multiple regions with negative phase shift obtained at 1 Hz and 2 Hz. (** indicates p-value less than 0.005).

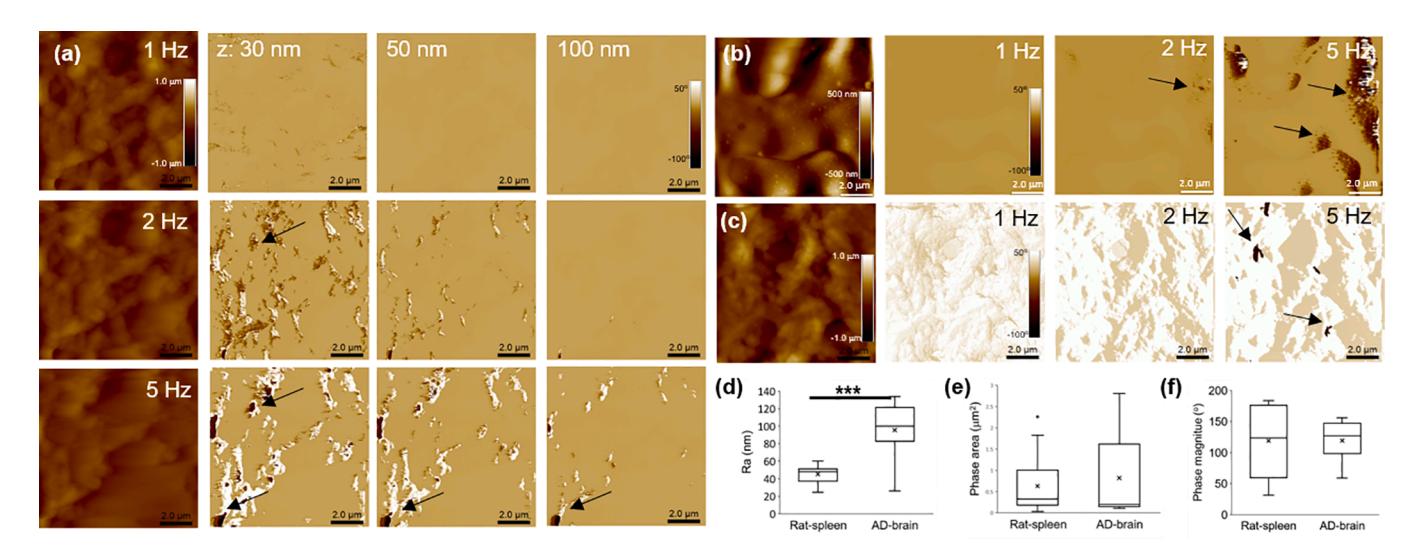


Fig. 2. (a) Scan rate dependent artifacts (arrows) in phase images of OCT-embedded brain tissue from a subject with Alzheimer's Disease (AD). The artifacts increase with increasing scan rates and persist even at a lift height (z) of 100 nm. Similar artifacts were observed in brain tissue from patients (b) without AD and (c) in AD brain tissue when scanned with a non-magnetic AFM probe at z=30 nm. Quantitative analysis comparing (d) topographical surface roughness from height images and (e) size (area) and (f) magnitude of negative phase obtained from rodent spleen and AD brain tissue (at 2 Hz and z=30 nm). (*** indicates p-value less than 0.001)

illustrated in Fig. 3a-b, we could obtain MFM images from region(s) which resembled macrophages surrounded by the polygonal shaped splenic red-pulp cells. The morphology of these regions was verified using TEM imaging (Fig. 3c) and Perls staining (inset) of adjacent sections. At the low scan rate of 1 Hz, MFM images predominantly consisted

of signals from subcellular organelles which resembled lysosomes in macrophages. However, at 2 Hz, artifacts (i.e. additional regions with negative phase shift) appeared, which were not present at 1 Hz. The surface roughness (R_a) of height images as well as the size and magnitude of the negative phase shift obtained at 2 Hz for resin sections, were

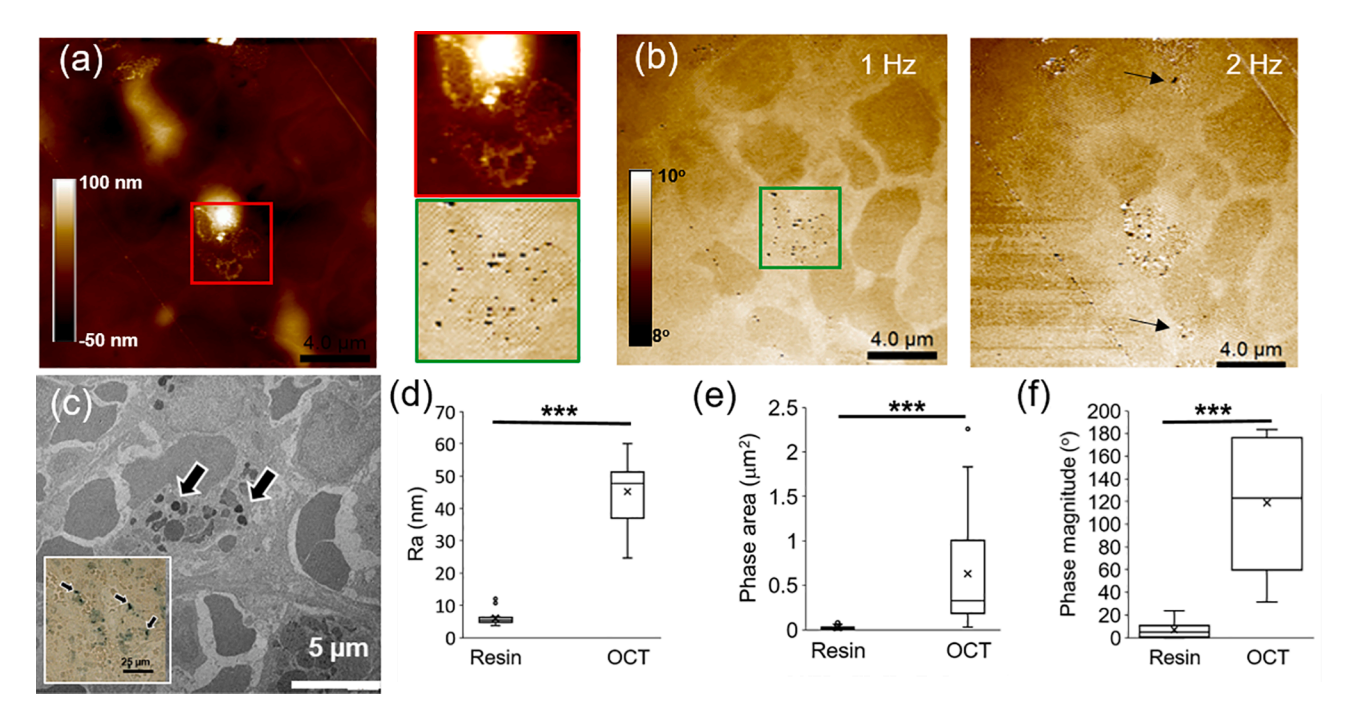


Fig. 3. (a) Sections of resin-embedded rodent spleen imaged using a MFM probe at a lift height z=30 nm and scan rates as indicated. Nanoscale sized regions with negative phase shift are observed at 1 Hz from a region corresponding to subcellular organelles in the height image. (b) Additional regions with negative phase shift (arrows) start appearing in phase images at scan rates of 2 Hz. (c) TEM image of an adjacent section shows similar morphology of splenic cells as observed in MFM images. Inset in (c) is Perls staining of an adjacent section showing presence of iron as blue stain (arrows). Quantitative analysis comparing (d) topographical surface roughness from height images and (e) size (area) and (f) magnitude of phase obtained from resin and OCT embedded sections of rodent spleen (at 2 Hz and z=30 nm). (*** indicates p-value less than 0.001).

significantly lower than those observed from the thicker OCT-embedded sections (Fig. 3d-f).

4. Discussion

One of the major challenges in MFM analysis is the contamination of MFM signal with artifacts arising due to topographical cross-talk, as has been shown for samples consisting of solid-state materials [26] or nanoparticles [27]. The cross-talk is understood to originate from capacitive coupling effects, topographical roughness and/or local changes in material properties of the sample. Several lines of investigations have been put forth to address the issue of cross-talk in MFM. Some of these approaches include reversal of MFM tip polarity [28], use of AC magnetic field [29], adopting a data fusion approach involving a combination of linear lift mode with interleave mode [30] and use of Kelvin probe force microscopy (KPFM) to discern the capacitive coupling effects in MFM experiments [31]. The issue of crosstalk in MFM of biological samples is even less investigated. Biological samples (e.g. histological sections) can add further complexity to topographical cross-talk due to heterogeneity in their composition, adhesive forces, and stiffness.

Previous studies by us [20,21] and others [32] utilized a low scan rate (1 Hz) for MFM of biological samples. At this low scan rates, we could detect features with negative phase shifts in an iron-rich tissue such as rodent spleen which corresponded to the size of ferritin(iron) rich lysosomes in splenic macrophages [20]. Nanoscale pathological iron has also been detected in the AD brain tissue by using X-ray absorption [33], analytical electron microscopy [34], or magnetic resonance microscopy [35]. The high magnetic moment of magnetite as compared to ferrihydrite (found in physiological ferritin) makes it an attractive material for MFM studies. Along these lines, in an earlier report, MFM signals were detected on very thick sections of the epileptic brain, which had been previously characterized for magnetic material via isothermal remnant magnetization [36]. We could not detect iron via

Perls staining in our AD samples, indicating that iron is heterogeneously distributed in the AD brain. Nevertheless, we experimented with both rodent spleen and AD brain tissue to elucidate how scan rate dependent artifacts appear in MFM images of tissues which are replete with as well those devoid of nanoscale iron deposits.

To circumvent the issue of scan-rate dependent artifacts in MFM analysis, we also examined samples with reduced surface roughness by using resin-embedded sections of rodent spleen. The frequency, size, and magnitude of the MFM signal (at 1 Hz) was diminished in these sections as compared to the thicker OCT embedded tissue. Nevertheless, the resin sections (with reduced sample roughness) also exhibited scan-rate dependent artifacts at 2 Hz.

Taken together, the presence of artifacts can make it difficult to discern true MFM signal (from iron-rich regions). While these artifacts can be minimized by restricting to low scan rates, it limits the efficiency of MFM experiments. Scan rate has been an important parameter for image quality in AFM. Although the visualization of topographic images may not differ drastically at high scan rates (as observed in our study), scan rate can impact parameters like aspect ratio, etc [37]. It is important to note that in interleave modes such as MFM, fast scan rate may also compromise the ability of the probe to quickly achieve the desired lift height at each sample point, which can result in artifacts [38]. The advancement of high-speed AFM or novel feedback mechanisms [26] may help overcome some of these limitations.

Recent years have witnessed advances in multimodal imaging involving MFM and electron microscopy approaches to unambiguously detect magnetic domains in magnetic recording media [39]. Along these lines we have also recently developed indirect magnetic force microscopy (ID-MFM) [40], as a multimodal technique. In ID-MFM the MFM signal can be detected from samples deposited on the underside of an ultrathin silicon—nitride membrane. ID-MFM is amenable to light microscopy and TEM and can eliminate artifacts due to topographical cross-talk thus providing a more accurate estimate of magnetic signals. Other emerging label-free magnetic imaging techniques include the

diamond nitrogen vacancy (NV) center approach as shown recently for ferritin in cells [41]. The evidence of artifacts in these emerging techniques remains to be examined.

CRediT authorship contribution statement

Kevin J. Walsh: Conceptualization, Data curation, Formal analysis, Methodology, Validation, Visualization, Writing - original draft, Writing - review & editing. Owen Shiflett: Data curation, Formal analysis, Visualization. Stavan V. Shah: Data curation, Formal analysis, Visualization, Writing - original draft. Theodore Renner: Methodology. Nicolas Soulas: Data curation, Formal analysis. Douglas Scharre: Resources. Dana M. McTigue: Funding acquisition, Resources. Gunjan Agarwal: Conceptualization, Data curation, Formal analysis, Funding acquisition, Investigation, Methodology, Resources, Software, Supervision, Validation, Visualization, Writing - original draft, Writing -review & editing

Declaration of Competing Interest

The authors declare that they have no known competing financial interests or personal relationships that could have appeared to influence the work reported in this paper.

Data availability

Data will be made available on request.

Acknowledgements

This work was supported in part by a seed grant (to GA and DM) from the Chronic Brain Injury program at The Ohio State University, by the NSF CBET 2038055 and NIH 1S10OD025096-01A1 awards (to GA) and a pre-doctoral fellowship (to KW) via the NIH T32 GM118291-01A1 award

References

- [1] N. Gálvez, B. Fernández, P. Sánchez, et al., Comparative structural and chemical studies of ferritin cores with gradual removal of their iron contents, J. Am. Chem. Soc. 130 (25) (2008) 8062–8068.
- [2] S.M. Dubiel, B. Zablotna-Rypien, J.B. Mackey, Magnetic properties of human liver and brain ferritin, Eur. Biophys. J. 28 (3) (1999) 263–267.
- [3] G. Agarwal, Characterization of Magnetic Nanomaterials Using Magnetic Force Microscopy, in: Magnetic Nanomaterials for Life Sciences, 2009.
- [4] E. Pinilla-Cienfuegos, S. Mañas-Valero, A. Forment-Aliaga, E. Coronado, Switching the Magnetic Vortex Core in a Single Nanoparticle, ACS. Nano. 10 (2) (2016) 1764–1770.
- [5] X. Batlle, C. Moya, N. Pérez, Ó. Iglesias-Freire, A. Asenjo, A. Labarta, Direct imaging of the magnetic polarity and reversal mechanism in individual Fe 3–x O 4 nanoparticles, Nanoscale. 7 (17) (2015) 8110–8114.
- [6] V.F. Puntes, P. Gorostiza, D.M. Aruguete, N.G. Bastus, A.P. Alivisatos, Collective behaviour in two-dimensional cobalt nanoparticle assemblies observed by magnetic force microscopy, Nat. Mater. 3 (4) (2004) 263–268.
- [7] S. Schreiber, M. Savla, D.V. Pelekhov, et al., Magnetic force microscopy of superparamagnetic nanoparticles, Small. 4 (2) (2008) 270–278.
- [8] S. Sievers, K.F. Braun, D. Eberbeck, et al., Quantitative measurement of the magnetic moment of individual magnetic nanoparticles by magnetic force microscopy, Small. 8 (17) (2012) 2675–2679.
- [9] T.M. Nocera, J. Chen, C.B. Murray, G. Agarwal, Magnetic anisotropy considerations in magnetic force microscopy studies of single superparamagnetic nanoparticles, Nanotechnology. 23 (49) (2012), 495704.
- [10] X. Li, Y. Xue, Q. Jia, F. Liu, Z. Li, Magnetic domains characterization of clusters of magnetite nanoparticles, Phys. E. Low-Dimensional. Syst. Nanostructures. (2019).
- [11] L. Angeloni, D. Passeri, S. Corsetti, D. Peddis, D. Mantovani, M. Rossi, Single nanoparticles magnetization curves by controlled tip magnetization magnetic force microscopy, Nanoscale. 9 (45) (2017) 18000–18011.
- [12] J.A. Fuentes-García, A.I. Diaz-Cano, A. Guillen-Cervantes, J. Santoyo-Salazar, Magnetic domain interactions of Fe3O4nanoparticles embedded in a SiO2matrix, Sci. Rep. 8 (1) (2018).

- [13] C. Moya, Ó. Iglesias-Freire, X. Batlle, A. Labarta, A. Asenjo, Superparamagnetic versus blocked states in aggregates of Fe3-xO4 nanoparticles studied by MFM, Nanoscale. 7 (42) (2015) 17764–17770.
- [14] D. Passeri, C. Dong, M. Reggente, et al., Magnetic force microscopy: quantitative issues in biomaterials, Biomatter. 4 (1) (2014) e29507.
- [15] S. Hsieh, C.W. Hsieh, B. Zheng, Ferritin protein imaging and detection by magnetic force microscopy, Chem. Commun. 46 (10) (2010) 1655–1657.
- [16] T.M. Nocera, Y. Zeng, G. Agarwal, Distinguishing ferritin from apoferritin using magnetic force microscopy, Nanotechnology. 25 (46) (2014), 461001.
- [17] K.J. Kim, H.Y. Cho, W.J. Lee, J.W. Choi, Subtyping of Magnetically Isolated Breast Cancer Cells Using Magnetic Force Microscopy, Biotechnol. J. 13 (6) (2018).
- [18] C.E. Diebel, R. Proksch, C.R. Green, P. Neilson, M.M. Walker, Magnetite defines a vertebrate magnetoreceptor, Nature. 406 (6793) (2000) 299–302.
 [19] C. Marcuello, L. Chambel, M.S. Rodrigues, L.P. Ferreira, M.M. Cruz, Magnetotactic
- [19] C. Marcuello, L. Chambel, M.S. Rodrigues, L.P. Ferreira, M.M. Cruz, Magnetotactic Bacteria: Magnetism beyond Magnetosomes, IEEE. Trans. Nanobioscience. 17 (4) (2018) 555–559.
- [20] A.R. Blissett, B. Ollander, B. Penn, D.M. McTigue, G. Agarwal, Magnetic mapping of iron in rodent spleen, Nanomedicine. Nanotechnology,. Biol. Med. 13 (3) (2017) 977–986.
- [21] A.R. Blissett, B. Deng, P. Wei, et al., Sub-cellular In-situ Characterization of Ferritin (iron) in a Rodent Model of Spinal Cord Injury, Sci. Rep. 8 (2018) 3567.
- [22] T.J. Montine, C.H. Phelps, T.G. Beach, et al., National institute on aging-Alzheimer's association guidelines for the neuropathologic assessment of Alzheimer's disease: A practical approach, Acta. Neuropathol. 123 (1) (2012) 1–11.
- [23] H. Braak, E. Braak, Staging of alzheimer's disease-related neurofibrillary changes, Neurobiol. Aging. 16 (3) (1995) 271–278.
- [24] Y. Tanaka, J.A. Berschauer, Application of the Perls method for iron staining to sections embedded in epoxy resin, Stain. Technol. 44 (5) (1969) 255–256.
- [25] B. Jones, A. Debski, C.P. Hans, M.R. Go, G. Agarwal, Structurally abnormal collagen fibrils in abdominal aortic aneurysm resist platelet adhesion, J. Thromb. Haemost. 20 (2) (2022) 470–477.
- [26] A. Moldovan, M. Dinescu, Single-pass magnetic force microscopy technique, with topography feedback based on scanning polarization force microscopy, Appl. Surf. Sci. 597 (2022), 153747.
- [27] L. Angeloni, D. Passeri, M. Reggente, D. Mantovani, M. Rossi, Removal of electrostatic artifacts in magnetic force microscopy by controlled magnetization of the tip: Application to superparamagnetic nanoparticles, Sci. Rep. 6 (April) (2016) 1–14.
- [28] L. Angeloni, D. Passeri, M. Reggente, D. Mantovani, M. Rossi, Removal of electrostatic artifacts in magnetic force microscopy by controlled magnetization of the tip: Application to superparamagnetic nanoparticles, Sci. Rep. (2016) 6.
- [29] Y. Cao, S. Nakayama, P. Kumar, et al., Magnetic domain structure imaging near sample surface with alternating magnetic force microscopy by using AC magnetic field modulated superparamagnetic tip, Nanotechnology. 29 (30) (2018).
- [30] M. Fuhrmann, A. Krivcov, A. Musyanovych, R. Thoelen, H. Möbius, The Role of Nanoparticles on Topographic Cross-Talk in Electric Force Microscopy and Magnetic Force Microscopy, Phys. Status. Solidi. Appl. Mater. Sci. 217 (13) (2020) 1–6.
- [31] C. Schönenberger, S.F. Alvarado, S.E. Lambert, I.L. Sanders, Separation of magnetic and topographic effects in force microscopy, J. Appl. Phys. 67 (12) (1990) 7278–7280.
- [32] M. Arredondo, M. Stoytcheva, I. Morales-Reyes, N. Batina, AFM and MFM techniques for enzyme activity imaging and quantification. http://mc. manuscriptcentral.com/tbeq. 2018;32(4):1065-1074.
- [33] Q. Pankhurst, D. Hautot, N. Khan, J. Dobson, Increased levels of magnetic iron compounds in Alzheimer's disease, J. Alzheimers. Dis. 13 (1) (2008) 49–52.
- [34] J.F. Collingwood, A. Mikhaylova, M. Davidson, et al., In situ characterization and mapping of iron compounds in Alzheimer's disease tissue, J. Alzheimer's. Dis. 7 (4) (2005) 267-272
- [35] V. Antharam, J.F. Collingwood, J.-P. Bullivant, et al., High field magnetic resonance microscopy of the human hippocampus in Alzheimer's disease: Quantitative imaging and correlation with iron, Neuroimage. 59 (2) (2012) 1249–1260
- [36] J.R. Dunn, M. Fuller, J. Zoeger, et al., Magnetic material in the human hippocampus, Brain. Res. Bull. 36 (2) (1995) 149–153.
- [37] F.M. Mwema, E.T. Akinlabi, O.P. Oladijo, Effect Of Scan Rate On AFM Imaging On 3D Surface Stereometrics Of Aluminum Films, Mater. Today. Proc. 18 (2019) 2315–2321.
- [38] L. Tang, Y. Bai, C. Duan, et al., Dynamic speed control in atomic force microscopy to improve imaging time and quality, Meas. Sci. Technol. 25 (4) (2014), 044005.
- [39] T.R. Kim, C. Phatak, A.K. Petford-Long, et al., Correlative magnetic imaging of heat-assisted magnetic recording media in cross section using lorentz TEM and MFM, IEEE. Trans. Magn. 54 (1) (2018).
- [40] J. Sifford, K.J. Walsh, S. Tong, G. Bao, G. Agarwal, Indirect magnetic force microscopy, Nanoscale. Adv. 1 (6) (2019) 2348–2355.
- [41] P. Wang, S. Chen, M. Guo, et al., Nanoscale magnetic imaging of ferritins in a single cell, Sci. Adv. 5 (4) (2019).